Available online at www.sciencedirect.com
SCIENCE DIRECT
Icarus 180 (2006) 265–273
ICARUS
www.elsevier.com/locate/icarus

Synthesis of hydrogen peroxide in water ice by ion irradiation

M.J. Loeffler [a,*], U. Raut [a], R.A. Vidal [a], R.A. Baragiola [a], R.W. Carlson [b]

[a] *University of Virginia, Laboratory for Atomic and Surface Physics, Thornton Hall B113, Charlottesville, VA 22904-4238, USA*
[b] *Jet Propulsion Laboratory, California Institute of Technology Pasadena, CA 91109, USA*

Received 17 May 2005; revised 20 July 2005

Available online 21 September 2005

Abstract

We present infrared absorption studies on the effects of 50–100 keV Ar^+ and 100 keV H^+ ion irradiation of water ice films at 20–120 K. The results support the view that energetic ions can produce hydrogen peroxide on the surface of icy satellites and rings in the outer Solar System, and on ice mantles on interstellar grains. The ion energies are characteristic of magnetospheric ions at Jupiter, and therefore the results support the idea that radiolysis by ion impact is the source of the H_2O_2 detected on Europa by the Galileo infrared spectrometer. We found that Ar^+ ions, used to mimic S^+ impacts, are roughly as efficient as H^+ ions in producing H_2O_2, and that 100 keV H^+ ions can produce hydrogen peroxide at 120 K. The synthesized hydrogen peroxide remained stable while warming the ice film after irradiation; the column density of the formed H_2O_2 is constant until the ice film begins to desorb, but the concentration of H_2O_2 increases with time during desorption because the water sublimes at a faster rate. Comparing the shape of the 3.5-μm absorption feature of H_2O_2 to the one measured on Europa shows excellent agreement in both shape and position, further indicating that the H_2O_2 detected on Europa is likely caused by radiolysis of water ice.

Keywords: Europa; Radiation chemistry; Infrared observations; Surfaces; Jupiter

1. Introduction

Most icy bodies in the outer Solar System and interstellar space have very thin atmospheres that cannot shield impacts of energetic particles and photons. Radiolytic products from these impacts, in particular those produced on typical water ice surfaces, can be detected from Earth and spacecraft by comparison of features in their optical reflectance spectra with those obtained in the laboratory. Our previous experimental studies have addressed the production mechanisms responsible for the observations of solid O_2 on the Galilean satellites (Vidal et al., 1997; Baragiola and Bahr, 1998; Baragiola et al., 1999a; Bahr et al., 2001) and O_3 on Ganymede, Rhea, and Dione (Baragiola et al., 1999b; Famá et al., 2002).

Here we report studies of the production of hydrogen peroxide by ion irradiation in vapor-deposited water ice at 20–120 K, which have been motivated by the detection of H_2O_2 on Europa (Carlson et al., 1999) using the Galileo NIMS infrared spectrometer. These observations, compared with infrared measurements of a solid solution of H_2O_2 in water, indicated a peroxide concentration of 0.13% on Europa's surface. The significance of those observations is that the presence of photolytically unstable H_2O_2 on Europa is considered to be an unambiguous indicator of radiation processing of the surface ice.

There have been a few previous laboratory studies to test the hypothesis that H_2O_2 on Europa is produced by ion irradiation of water ice, but the results appear to be contradictory. Moore and Hudson (2000) observed the 3.5-μm infrared band of H_2O_2 after irradiation of water at 16 K with 800 keV protons. However, they saw no evidence for H_2O_2 when irradiating at 80 K, a temperature typical of cold regions on Europa, unless the ice also contained other molecules like O_2 or CO_2. Supporting those observations were experiments of Bahr et al. (2001) that detected only minute amounts of H_2O_2 by mass spectrometry when desorbing a pure ice film that had been irradiated by 200 keV protons at 80 and 120 K. The concentration detected, ∼0.001–0.02%, was below the detection limit of the IR absorption experiments. However, we now know that those values were greatly underestimated, perhaps by as much as two

* Corresponding author.
E-mail address: mjl8r@virginia.edu (M.J. Loeffler).

0019-1035/$ – see front matter
doi:10.1016/j.icarus.2005.08.001

orders of magnitude, because the extremely reactive H_2O_2 is destroyed in collisions with the vacuum chamber walls before detection and is strongly fractioned in the mass spectrometer. Gomis et al. (2004a) performed infrared experiments similar to those of Moore and Hudson (2000), but using lower energy (30 keV) protons and heavy ions. In contrast to the results of Moore and Hudson, they found that protons could produce H_2O_2 at 77 K in pure water ice, and even more abundantly than at 16 K whereas there was no temperature dependence in H_2O_2 production by Ar irradiation. Recently, Gomis et al. (2004b) published more studies on the formation of hydrogen peroxide with 200 keV H^+ and He^+ and 400 keV Ar^{++} ions, finding that the H_2O_2 saturation concentration is higher at lower temperatures for all three ions (saturation for 400 keV Ar^{++} at 16 K was an estimate (O. Gomis, private communication)). The higher value found in the 400 keV Ar^{++} experiments was associated to a hypothesized higher efficiency for radiation synthesis in elastic ion–water collisions that are important for Ar projectiles. However, the fact that H_2O_2 was produced in their 200 keV proton experiment at 77 K, but not by the 800 keV protons in Moore and Hudson's experiment at 80 K, could not be explained since, in both cases, electronic excitations vastly dominate energy deposition. Adding to this picture is the recent finding that low energy electrons, which only produce electronic excitations, can synthesize H_2O_2 at 87 K (Pan et al., 2004). These authors, using a mass spectrometry method similar to that of Bahr et al. (2001), found desorption of H_2O_2 and HO_2 from irradiated ice estimating that 19 eV electrons produced a surface concentration of $\lesssim$0.4%. These experiments are relevant to the discussion because such low energy electrons are produced abundantly during keV and MeV ion irradiation. One must note that in thermal desorption experiments the observed molecules might not exist in the as-irradiated film, but could result from the recombination of radicals induced by heating.

To contribute to the solution of this problem, we conducted infrared reflection absorption (IRRAS) studies of H_2O_2 synthesis by two different ions, H^+ and Ar^+, at two different energies, 50 and 100 keV, over a wider temperature range, 20–120 K. We used Ar^+ ions in addition to H^+ ions, because even though H^+ is the dominant magnetospheric ion on Europa, both sulfur and oxygen ions are also abundant (Paranicas et al., 2002). Furthermore, we used the 50–100 keV energies to simulate ion fluxes on Europa, which show broad distributions with maxima occurring at about 100 keV (Paranicas et al., 2002).

Our infrared studies included the dependence of the H_2O_2 column density on irradiation fluence at 20 and 80 K, on irradiation temperature between 20 and 120 K and on thermal desorption of the ice films. We present a method that enabled us to quantify absolute concentrations of molecules grown in a mixture, and an analysis of baseline subtraction on the 3.5-μm infrared absorption band, a difficult problem due to the proximity of the much stronger water OH stretch band. Furthermore, we show that the non-linear baseline subtraction enables us to characterize the shape of the 3.5-μm absorption feature, allowing the comparison of our results to the reflectance spectrum of Europa.

2. Experimental setup

All experiments were performed in a stainless steel vacuum chamber (Fig. 1) on a radiation-shielded cryostat. The base pressure of the chamber was 1×10^{-9} Torr and 1–2 orders of magnitude lower inside the shield. Water ice films were grown by vapor deposition on the gold mirror electrode of a quartz-crystal microbalance (QCM) that measures accurately the mass deposited per unit area, which can be converted to film column density (molecules cm^{-2} or thickness if the density is known) (Sack and Baragiola, 1993). Water vapor transported through a microcapillary array gas doser was incident at 5 degrees to the surface normal. All ice films were grown at a rate of ~45 nm min^{-1}. The growth temperature was 80 K except for the irradiations at 120 K where the films were grown at 120 K. In both conditions the ice was amorphous, as confirmed by infrared spectroscopy. The film thickness (1–1.9 μm) was chosen to be larger than the maximum ion ranges (Ziegler, 2003) to avoid altering the Au mirror with the ion beam. Thus, except for a negligible backscattered fraction, the ions deposit all their energy in the film. In terms of column density η, we used films with $\eta \approx 2.8 \times 10^{18}$ H_2O cm^{-2} for the 50 keV and 100 keV Ar^+ irradiations and $\eta \approx 5.2 \times 10^{18}$ H_2O cm^{-2} for the 100 keV H^+ irradiations. The ion beams were produced by an ion accelerator, mass analyzed and scanned uniformly over the target, while the beam current density was monitored in real time by a calibrated thin wire collector, placed in the ion beam path.

The specular infrared reflectance of the films on the gold mirror was measured at an incident angle of 45° with a Thermo-Nicolet Nexus 670 Fourier Transform infrared spectrometer at 2-cm^{-1} resolution. The spectra were divided by the spectrum of the gold mirror substrate taken before ice deposition. The ratios R were then converted to optical depth units: $-\ln(R)$, and the band area was quantified by subtracting a non-linear baseline (background) under the 3.5-μm H_2O_2 band and dividing by the path length of the infrared beam (2.28, using $n = 1.45$). The subtraction is made difficult because the baseline, which is due

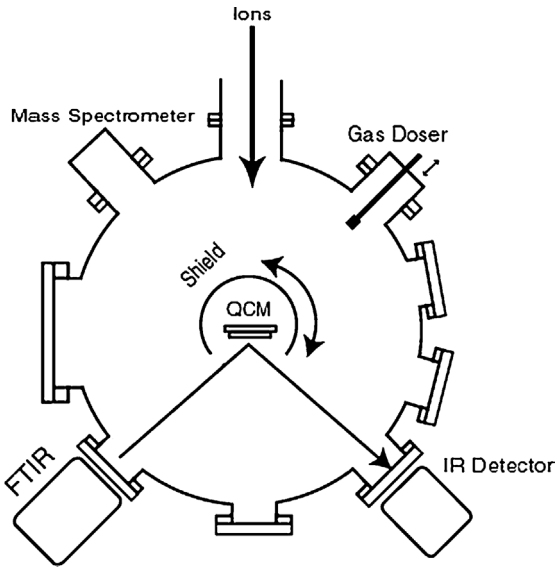

Fig. 1. The experimental setup.

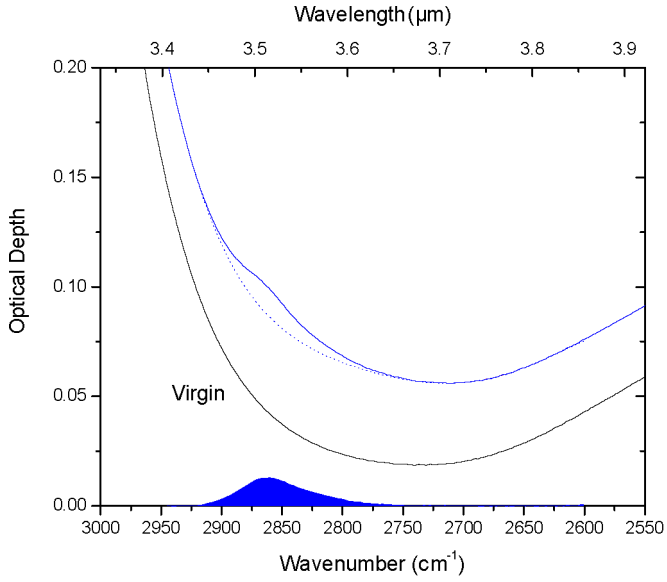

Fig. 2. An example of the baseline fit for the H_2O_2 region for the irradiation of 5.2×10^{18} H_2O molecules cm^{-2} at 80 K with 100 keV H^+ at a fluence of 2.7×10^{15} ions cm^{-2}.

to absorption by the O–H stretch in water, is very strong and curved. Thus, it is important to go beyond the straight-line approximation used in previous studies, to avoid underestimating the band area. We used a polynomial fit with a shape similar to that of the spectrum of virgin ice, to ensure that the baseline is physically reasonable, besides giving a mathematical fit without introducing additional structures (Fig. 2). Also, in some cases we compared the derivatives of the unirradiated spectra, irradiated spectra and the baseline to ensure the shape of the fit was adequate and that no spurious structures were added. At low irradiation fluence, F (ions cm^{-2}), where the H_2O_2 concentrations are very small, the mathematical fit is ambiguous and was not used. Since at these fluences the change of the water OH band with irradiation is very small, we subtracted, in optical depth units, the irradiated spectrum from the virgin ice. This method enabled us to quantify small H_2O_2 band areas necessary to study the initial dependence on irradiation fluence.

To convert band areas to column densities we need to divide them by the band absorption strength. However, we need to account also for interference effects that affect all thin film experiments in IRRAS. We do this by using an *effective* band strength, A_t, for films of the same thickness. This quantity was measured by co-depositing, with two gas dosers, H_2O_2 and water at 110 K into a sandwich of an H_2O_2:H_2O mixture surrounded by pure water. This calibration was done for the two thicknesses used in these experiments (we use the thickness after irradiation, which is slightly different to that of the as-deposited films due to sputtering and compaction). The H_2O_2 used for the deposition was of >97% purity prepared by vacuum distillation of a 50% solution of H_2O_2; more details will be given in a future paper. The two gases were controlled independently by separate gas dosers with a deposition rate for each one determined separately with the microbalance to produce mixed ice films with the desired H_2O_2 concentration (<5%). The relatively high growth temperature was chosen so that impurities, formed when H_2O_2 reacts with the chamber walls, would not stick on the substrate. We measured the infrared reflectance of the films and calculated the area of the 3.5-μm absorption band in optical depth units. After accounting for the temperature dependence of the band strength and dividing by the path length of the infrared beam, we find, e.g., at 20 K, $A_t = 6.5 \times 10^{-17}$ cm molecule^{-1} for a 1.9-μm film and 8.7×10^{-17} cm molecule^{-1} for a 1-μm film. The thickness dependence of A_t observed in these mixtures is a consequence of optical interference effects in thin films, described by the Fresnel equations in terms of the optical constants of the substrate and the film. We note that these interference effects are the same for irradiated films, since the thickness is the same, and since roughness effects are insignificant at the fluence used.

To compare our results to previous infrared transmission studies, we need to obtain the absolute band strength A. We do this iteratively using the Fresnel equations with a Kramers–Kronig analysis of the spectra to optimize the optical constants for our mixtures. The only parameter we estimate in our experiments is the density of the films to obtain the thickness from the areal mass given by the QCM; this is quite accurate since the concentration of H_2O_2 is very low. We apply the rule of mixtures, with the known column densities of water and hydrogen peroxide in the films; the density of water and hydrogen peroxide (1.6 g cm^{-3}) were measured by the technique of Westley et al. (1998). We arrive at a density of (0.94 ± 0.02) g cm^{-3}, which yields $A = (5.7 \pm 0.6) \times 10^{-17}$ cm molecule^{-1} for H_2O_2 dispersed in a water environment at 20 K. We noted a slight temperature dependence: $A = (5.2 \pm 0.6) \times 10^{-17}$ cm molecule^{-1} at 80 K and $(4.9 \pm 0.5) \times 10^{-17}$ cm molecule^{-1} at 110 K. We note that the values for A are about twice as large as that used by Gomis et al. (2004a, 2004b).

3. Results

3.1. Fluence dependence of H_2O_2 production

We irradiated water ice at normal incidence with 100 keV H^+ at 20 and 80 K, obtaining the fluence dependences of H_2O_2 column density, $\eta(F)$, shown in Fig. 3. At 80 K the initial production rate is clearly linear whereas for 20 K the uncertainty is such that we cannot rule out a quadratic component.[1] In any event, the initial production rate is lower at higher temperatures, suggesting that a key mechanism involved in H_2O_2 production at 20 K is suppressed at 80 K. At large fluences, $\eta(F)$ saturates to a value that we denote by η_∞, which is ~5 times larger at 20 than at 80 K. To compare with observations on Europa we obtain averaged H_2O_2 concentrations by dividing the column densities of H_2O_2 by that of water over the penetration range of the ions, calculated with the Monte Carlo code SRIM 2003 (Ziegler, 2003). We find that the concentration at 80 K, 0.14% (Table 1), is quite close to the value observed on Europa.

[1] In the lower temperature experiments, the H_2O_2 band appeared at longer wavelengths, slightly overlapping the 4.5-μm band of water ice. This increased the uncertainty in the fit to the tail of the absorption; this uncertainty may explain the slight increase in the width measured at 20 verses 80 K (see Figs. 8 and 9).

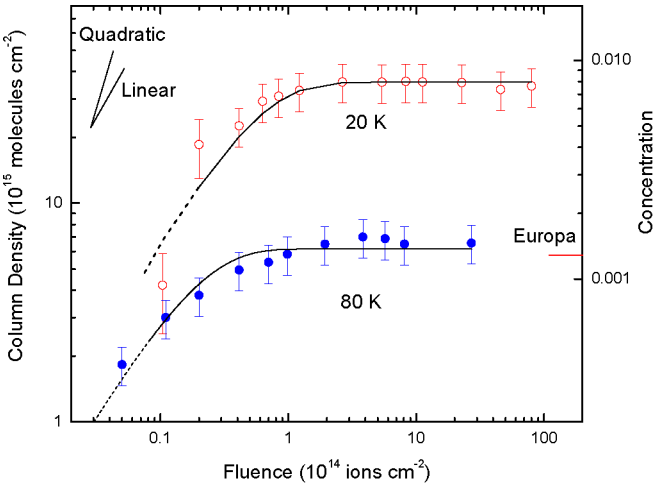

Fig. 3. Fluence dependence of the H_2O_2 column density at 20 and 80 K for 100 keV H^+ irradiation of amorphous water ice. The dotted and solid line together show the fit to the data, using Eq. (15); the dotted part indicates the initial rise. The right axis shows average concentration over the penetration range of the ion, and the average on Europa from Carlson et al. (1999).

Table 1
Parameters from fits of Eq. (15) to fluence dependence for a film of water $\eta = 5.2 \times 10^{18}$ H_2O cm^{-2} thick irradiated with 100 keV H^+ ions

	σ_c (10^{-16} cm^2)	σ_d (10^{-14} cm^2)	$C_\infty \times 100$	G
20 K	1.4 ± 0.2	2.0 ± 0.3	0.75 ± 0.15	0.72*
80 K	0.69 ± 0.03	5.9 ± 0.6	0.14 ± 0.03	0.36 ± 0.03

C_∞ is the H_2O_2 concentration measured at saturation for the 100 keV H^+ ions.
* Upper bound due to uncertainty in the existence of a quadratic component.

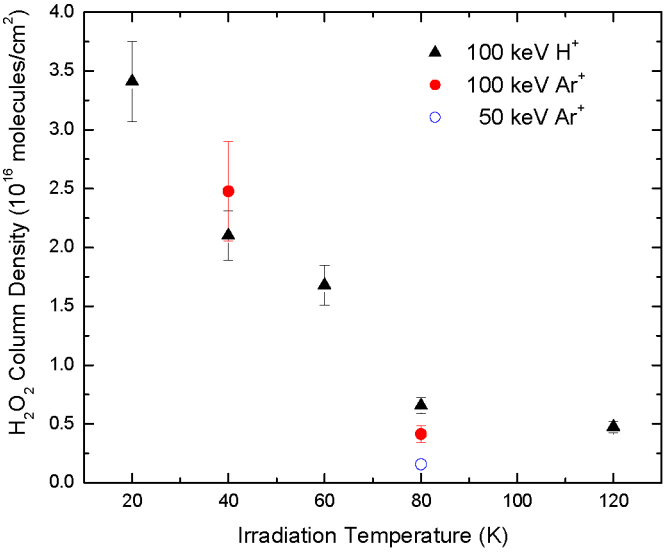

Fig. 4. Saturation values of the H_2O_2 column density produced by 100 keV H^+ incident on 5.2×10^{18} H_2O molecules cm^{-2} films, and by 50 and 100 keV Ar^+ incident on 2.8×10^{18} H_2O molecules cm^{-2} films.

We show in Fig. 4 the values of η_∞ for Ar^+ and H^+ ions in the range 20–120 K, where one can see that more H_2O_2 is produced at lower temperatures, in agreement with the data of Moore and Hudson (2000) for 800 keV protons,

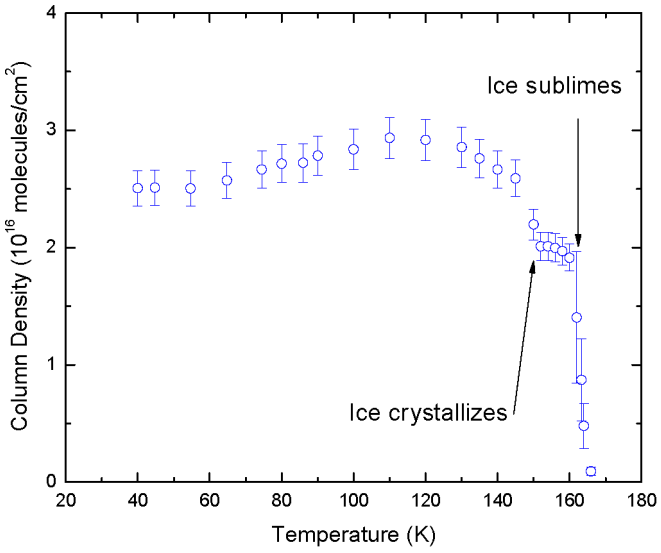

Fig. 5. H_2O_2 column density as a function of annealing temperature for a 2.8×10^{18} H_2O molecules cm^{-2} water ice film irradiated by 100 keV Ar^+ ions at 40 K. The large error bars at the higher temperatures are due to uncertainties in the change of band strength with film thickness as the film evaporates.

except that we can observe H_2O_2 at 120 K for higher fluence values ($\sim 10^{14}$ ions cm^{-2}), which was undetectable in their case at 80 K. The temperature dependence of our result is in general agreement with that reported by Gomis et al. for 200 keV protons and He^+, but not with that reported for 30 keV protons. We find for 100 keV Ar^+ that more peroxide is formed at the lower temperatures; this agrees with the results for 400 keV Ar^{++} estimated by Gomis et al. (2004b) but not with their 30 keV Ar^+ data (Gomis et al., 2004a) that showed no temperature dependence. Also noteworthy in Fig. 4 is that, at 80 K, η_∞ for Ar^+ is more than double at 100 than at 50 keV. It can be seen that 100 keV Ar^+ produce similar η_∞ as 100 keV protons at 40 K, but ~50% less at 80 K. We note that, if instead of using the total amount of radiation products, as is standard procedure in radiation chemistry, we consider *concentrations*, we obtain that this quantity is much higher for Ar^+ than for H^+, due to the shorter penetration depth.

3.2. Position and stability of the H_2O_2 absorption feature

After reaching saturation at various temperatures we warmed the irradiated films to see whether the H_2O_2 absorption band changed with temperature. We found that η remained relatively constant until the film began to desorb from the gold substrate (Fig. 5). The slight variation with temperature may be caused by reactions with radicals trapped in the ice. Since during desorption water ice sublimes faster than the peroxide, the concentration of H_2O_2 is enhanced (Fig. 6). Furthermore, after background subtraction the H_2O_2 band position increases slightly in frequency while increasing the temperature to 120 K. We observed a similar behavior for an H_2O_2:H_2O mixture grown at 16 K. A new finding is that this annealing process creates an irreversible change in the amorphous film and there-

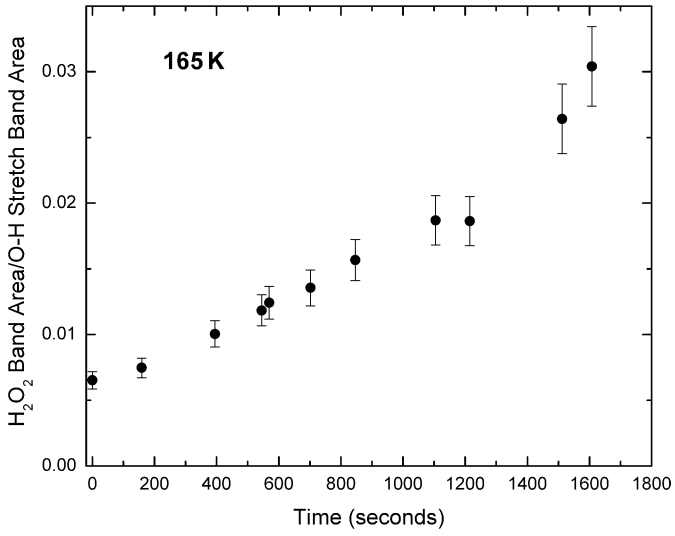

Fig. 6. Relative band areas for the 3.5-μm H_2O_2 band and the 3.1-μm OH-stretch band of water and H_2O_2 as the film sublimes at 165 K.

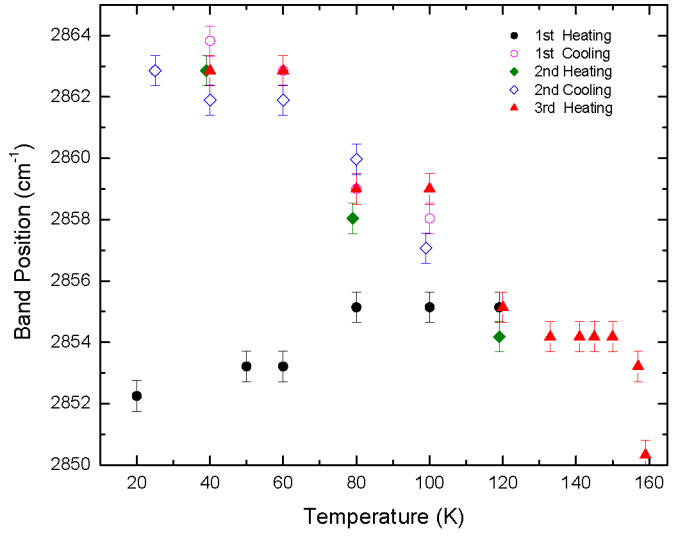

Fig. 7. The peak frequency of the 3.5-μm H_2O_2 absorption band vs temperature for a water ice film irradiated with 100 keV H^+ ions at 20 K. For comparison, the position of the band on Europa has been reported to be at 2857 cm^{-1} (Carlson et al., 1999).

after, the band position follows a different, and reversible, temperature curve (Fig. 7), increasing when cooling. This reversible behavior was also seen in crystalline mixtures grown at ∼150 K.

Finally, we found an interesting change in the band shape as we cool irradiated films that have been annealed to 120 K: a shoulder appears in the low frequency side of the band (Fig. 8). This behavior is reversible, that is, the shoulder disappears when heating and reappears when cooling. The shoulder might indicate the presence of two absorptions in the 3.5-μm band (multiple overtones and/or a combination mode) or may signal the presence of a doublet, known to occur in H_2O_2 due to symmetry (Hougen, 1984; Pettersson et al., 1997).

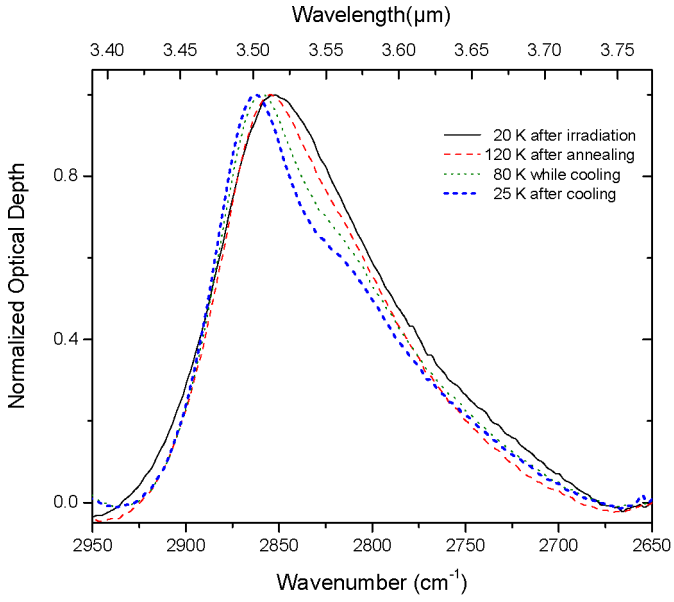

Fig. 8. Changes in the hydrogen peroxide band as the temperature of film is varied for an initially 5.2×10^{18} H_2O molecules cm^{-2} water ice film, irradiated with 100 keV H^+ ions until saturation. The shoulder appearing at short frequencies is only seen at low temperatures after the film has been annealed to 120 K.

4. Discussion

4.1. Comparison to other experiments

An evaluation of the general concepts learned from irradiation of water by fast particles may be useful for gaining insight into radiation experiments performed on ices. We can calculate the initial (low-fluence limit) radiation yield G, defined as the number of molecules produced per 100 eV of deposited energy. In our case, where the ions deposit all their energy E_0 in the film, the radiation yield is an average over the penetration depth: $G = \mathrm{d}(\eta(F))/\mathrm{d}F \times 100\ \mathrm{eV}/E_0$. We can calculate G more accurately for the 80 K data where an initial linear slope is clear in the $\eta(F)$ curve. The derived values are shown in Table 1.

We now turn our attention to the fact that, among the experiments that have investigated in situ H_2O_2 production in water ice at ∼80 K, peroxide was not detected for 800 keV protons. This can be explained by the fact that those projectiles cause a low density of excitations/ionizations due to their low linear energy transfer (LET or energy deposited per unit path length dx). The LET can be approximated by the stopping power of the projectile, dE/dx, since the fraction of energy that escapes with ejected electrons, photons, and atomic particles is negligible. It is known that the relative yield of molecular species (such as O_2 and H_2O_2) increases with LET in liquid water and water solutions (Hochanadel, 1960; Anbar, 1968; Spinks and Woods, 1990) and in ices (Hart and Platzman, 1961), but is in general independent of the type of incident particle, though exceptions have been found between light and heavy ions of the same LET (Wasselin-Trupin et al., 2002). We next discuss saturation concentrations, which appear to be higher for the projectile with highest LET.

We start by considering individual mechanisms in a simplified manner, since there are dozens of reactions involving different ion species and the neutral radicals H, O, OH, and HO_2. Although the reaction chemistry of water is well known in the gas phase, the lack of reaction rates in ice at low temperatures makes modeling unadvisable. A specific mechanism in the condensed state is the cage effect, where separating fragments of a dissociation collision bounce from adjacent molecules (the "cage"), slow down by momentum transfer and recombine with high probability. Because of momentum conservation, the lightest dissociation fragment (say H in a H–OH) carries most of the repulsive energy and is more likely to escape the cage. The cage opens transiently at the higher temperatures due to lattice vibrations causing escape to increase with temperature. Another condensed state effect are the much higher likelihood of three-body collisions compared with the gas phase, allowing reactions that would be forbidden in two-body collisions. A further concept needed to understand radiolysis of ice is that strong hydrogen bonds hinder diffusion of radicals, and results in their strong bonding at vacancies and other defects.

We now discuss the radiation effects on ice, limiting the discussion to representative processes involving the most abundant species. Radiolysis starts with excitations and ionizations described as follows, where X denotes an incident particle or photon:

$$\mathrm{X} + \mathrm{H_2O} \rightarrow \mathrm{H_2O^*}, \tag{1}$$

$$\rightarrow \mathrm{H_2O^+} + \mathrm{e^-}. \tag{2}$$

Almost nothing is known about the fate of the excited water molecule H_2O^*, besides that it will eventually relax to the ground state or dissociate, most likely to

$$\mathrm{H_2O^*} \rightarrow \mathrm{OH} + \mathrm{H}. \tag{3}$$

The ionized water molecule is thought to associate into hydronium in the reaction:

$$\mathrm{H_2O^+} + \mathrm{H_2O} \rightarrow \mathrm{H_3O^+} + \mathrm{OH}. \tag{4}$$

An unbound electron may recombine with the hydronium ion to form $H + H_2O$

$$\mathrm{e^-} + \mathrm{H_3O^+} \rightarrow \mathrm{H_2O} + \mathrm{H} \tag{5}$$

attach to an OH to form OH^-:

$$\mathrm{e^-} + \mathrm{OH} \rightarrow \mathrm{OH^-} \tag{6}$$

or to a water molecule by dissociative electron attachment (DEA):

$$\mathrm{e^-} + \mathrm{H_2O} \rightarrow \mathrm{OH^-} + \mathrm{H}. \tag{7}$$

The hydronium can also recombine with the negative hydroxyl radical to reform water molecules but releasing kinetic energy:

$$\mathrm{H_3O^+} + \mathrm{OH^-} \rightarrow 2\mathrm{H_2O}. \tag{8}$$

The OH that is not consumed in those reactions may react to form peroxide:

$$2\mathrm{OH} \rightarrow \mathrm{H_2O_2}. \tag{9}$$

We first consider the case of temperatures below 80 K, where OH diffusion is negligible (Siegel et al., 1961; Bednarek and Plonka, 1987). The two hydroxyl radicals in reaction (9) can be produced in an ion track of high LET caused by an ion, and this explains the apparent linear fluence dependence of the production rate we observe in the case of ion irradiation. On the other hand, low LET radiation such as photons produces isolated OH and, in the absence of diffusion, leads to a square dependence of H_2O_2 production on irradiation fluence, as observed for Lyman-α photons (Gerakines et al., 1996).

When temperature increases, the OH produced in the ion track can diffuse out before reaction (9) takes place. The resulting effect will be a decrease in the initial production rate, as seen at 80 K (Fig. 3). The ability of OH to diffuse out of the track before reacting with another radical will be larger if the initial OH concentration in the track is lower. This can explain why H_2O_2 was undetectable in the low LET experiments of Moore and Hudson (2000).

Another pathway for the formation of H_2O_2 starts with the formation of O:

$$\mathrm{X} + \mathrm{H_2O} \rightarrow \mathrm{H_2O^*} \rightarrow \mathrm{H_2} + \mathrm{O}. \tag{10}$$

This process accounts for 10% of the dissociations in the gas phase (Slanger and Black, 1982) but may be less likely in the solid due to the cage effect (for H_2 it should be more difficult to escape the cage than for H from (3)). Subsequent reactions in the ion track between two O atoms may lead to O_2:

$$\mathrm{O} + \mathrm{O} \rightarrow \mathrm{O_2}. \tag{11}$$

Alternatively, the O atom may be trapped at a defect site:

$$\mathrm{H_2O} + \mathrm{O} \rightarrow \mathrm{H_2O{-}O}. \tag{12}$$

Experimental evidence for reaction 12 in rare gas matrices has been reported by Khriachtchev et al. (2000), who showed that after forming a complex of H_2O–O by UV photolysis (193 nm) of H_2O_2, by photolysis at a different wavelength ($\lambda > 300$ nm) can then reform H_2O_2 by

$$\mathrm{X} + \mathrm{H_2O{-}O} \rightarrow \mathrm{H_2O^+} + \mathrm{O^-} \rightarrow \mathrm{H_2O_2}. \tag{13}$$

However, this mechanism for H_2O_2 formation implies a quadratic dependence on irradiation fluence, since one collision is needed in (10) and another in (13). This is not seen for ions, at least at 80 K, suggesting that process (9) in the ion track is more important for the formation of H_2O_2. The reason may be that the H_2O–O complex seen embedded in an inert rare gas solid matrix does not exist in a hydrogen-bonded medium such as water or H_2O_2.

A simple model for the fluence dependence assumes two processes, one to create H_2O_2 and one to destroy it, with effective cross sections σ_c and σ_d, respectively. Neglecting changes in the concentration of water, $[H_2O]$, we can write the rate equation:

$$\mathrm{d}[\mathrm{H_2O_2}]/\mathrm{d}F = \sigma_c[\mathrm{H_2O}] - \sigma_d[\mathrm{H_2O_2}], \tag{14}$$

which integrates to

$$C = (\sigma_c/\sigma_d)\big(1 - \exp(-\sigma_d F)\big), \tag{15}$$

where $C = [H_2O_2]/[H_2O]$. The saturation concentration is given by

$$C_\infty = \sigma_c/\sigma_d. \quad (16)$$

The values of σ_c and σ_d obtained by fitting the proton data to Eq. (15) are given in Table 1. We see that the values of the destruction cross section σ_d at 20 and 80 K are large, $\sigma_d \sim 2.0$–5.9×10^{-14} cm^2, respectively, significantly higher than previously assumed (Carlson et al., 1999). Both values are much larger than geometric cross sections, implying that, in addition to direct processes, the molecules can be destroyed by secondary processes involving other particles, such as electrons or radicals. Electrons can destroy H_2O_2 either by direct dissociation or by dissociative electron attachment:

$$e^- + H_2O_2 \rightarrow OH^- + OH, \quad (17)$$

$$e^- + H_2O_2 \rightarrow O^- + H_2O. \quad (18)$$

DEA is expected to be in the 10^{-16} cm^2 range in the gas phase (Nandi et al., 2003) but the reactions (17) and (18) are hindered in the solid by the cage effect. Since the number of ionizations are smaller than dissociations, because of the larger energy involved, it seems unlikely that electrons can account for the high effective cross section. To appreciate this more quantitatively, we include the cascade of all secondary electrons in the standard way by writing the effective cross section as $\sigma_d = S/J$, where S is the stopping power and J the mean energy to destroy H_2O_2. Since $S = 2.6 \times 10^{-14}$ eV cm^2 molecule^{-1} (Ziegler, 2003), using our measured σ_d we obtain $J \sim 1$ eV, but this value is much too small, smaller than the 2.1 eV dissociation energy of H_2O_2 into 2OH (Okabe, 1978). Thus, even though H_2O_2 production increases in water ice when electron scavengers are added (Moore and Hudson, 2000), another more dominant mechanism appears responsible for the large destruction cross section measured.

Another secondary process is afforded by reactions with radicals. In particular, other OH radicals produced in the water from reactions: (3), (4), and (7) can also destroy H_2O_2:

$$OH + H_2O_2 \rightarrow H_2O + HO_2 \quad (19)$$

and in turn, the HO_2 molecule formed can be destroyed by another OH producing water and molecular oxygen

$$OH + HO_2 \rightarrow H_2O + O_2. \quad (20)$$

Many other reactions with radicals can also destroy hydrogen peroxide (Luñák and Sedlák, 1992; Pastina and LaVerne, 2001; Alam et al., 2004), of which the most important are thought to be those involving H, an abundant radiolytic product:

$$H + H_2O_2 \rightarrow OH + H_2O, \quad (21)$$

$$H + H_2O_2 \rightarrow H_2 + HO_2. \quad (22)$$

To explain the increase in the effective destruction cross section with temperature we need to consider the behavior of the main radicals H and OH. Even at low temperatures, most of the OH will recombine with atomic hydrogen, which can diffuse even at the lowest temperatures used in these experiments and reform water. Some H will recombine with another H to form H_2 that diffuses out of the solid. Defects, intrinsic or produced by radiolysis will trap H and some H_2. At temperatures near or above 100 K, OH will diffuse and H may be released from traps, leading to additional OH–H recombination, which causes the well-known decrease of OH concentration with temperature (Plonka et al., 1984). Some of the diffusing H and OH will destroy hydrogen peroxide by reactions (19), (21) and (22), explaining the larger σ_d at the higher temperatures.

4.2. Comparison to Europa observations

Galileo infrared and ultraviolet spectra show the presence of hydrogen peroxide on Europa's leading hemisphere (Carlson et al., 1999). The H_2O_2 density varies over the surface and appears to correlate with surficial CO_2; however there are areas with relatively high concentrations of H_2O_2 and little CO_2 (Carlson, 2001). Hydrogen peroxide is not evident on the trailing hemisphere, but this lack of detection may be due to the high radiation noise associated with most Galileo NIMS Europa measurements. A related radiolytic species, O_2, is found at all longitudes on Europa (Spencer and Calvin, 2002), and if this O_2 is derived from H_2O_2 precursor (Sieger et al., 1998; Cooper et al., 2003; Johnson et al., 2003), then peroxide is expected to be on the trailing side as well.

Energetic particles striking Europa's surface include electrons, protons, iogenic sulfur and oxygen ions, and other ions in minor quantities. Electrons are thought to strike mainly the trailing side (Paranicas et al., 2001) while energetic ions, with their large gyroradii, bombard leading and trailing hemispheres with nearly equal intensity. The dominant ion species, in both number flux and energy flux, is protons and the peak in their flux distribution occurs at ∼100 keV (Paranicas et al., 2001). Europa's sulfur and oxygen ion fluxes are ∼20 and 10% of the proton flux at 100 keV (Paranicas et al., 2002). Thus, Europa's leading side H_2O_2 probably arises mainly from proton irradiation with energies of order 100 keV. There will also be a contribution from heavy ions but in the following we consider only protons and use the H^+ impact data described above for comparison.

The observed molar concentration on Europa is 0.13%, which agrees well with the measured equilibrium concentrations of 0.14 and 0.1% for H^+ irradiation at 80 K and 120 K (cf. Figs. 3 and 4). The experimental temperatures are relevant to Europa, for which average night and day temperatures at mid-latitudes are ∼90 and 120 K, respectively, estimated from (Spencer et al., 1999). The depth of penetration of 100 keV protons is just on the order of a 1–2 μm whereas the depth sampled by infrared remote sensing is probably tens of microns. Ions lose much of their energy at the ends of the tracks; thus higher energy ions can produce H_2O_2 as in the 100 keV case studied here, but deeper in the ice, which could be on the order of millimeters (Cooper et al., 2001; Paranicas et al., 2002). In addition, gardening by micrometeoroid impact will bury surficial peroxide molecules and may destroy some through vaporization. The average burial rate is about 1.2 μm year^{-1} (Cooper et al., 2001) but the rate will be greater on the leading side due to the enhanced flux from orbital

motion (Zahnle et al., 1998). Assuming that the sampling depth is 30 μm, and with an enhancement of 2.5 in the gardening rate at the leading apex (relative to the global average (Zahnle et al., 1998)), the observed layer has a gardening age of about 10 years.

Using the destruction cross section for 80 K (Table 1), the destruction rate per H_2O_2 molecule in the top few μm is $\sigma_d F = 8.9 \times 10^{-7}$ s^{-1} for the proton flux at Europa $F = 1.5 \times 10^7$ cm^{-2} s^{-1} (Cooper et al., 2001). This rate corresponds to a characteristic time of $\tau \sim 13$ days. The diurnally averaged photo-destruction rate for H_2O_2 at 5.2 AU is 2.5×10^{-6} s^{-1} (Huebner et al., 1992) in the gas phase but it is unknown and difficult to estimate in the solid phase. The absorption cross section for aqueous solutions of H_2O_2 is a factor of two greater than for gaseous H_2O_2 in the relevant spectral region (Lin et al., 1978) but the cage effect (see above) can reduce the net photo-destruction rate. For instance, in water, the radiolytic destruction rate of H_2O is one order of magnitude lower at 77 K than for the vapor (Spinks and Woods, 1990). In dilute mixtures in water, H_2O_2 may be even harder to dissociate than H_2O, because the two OH, which are the main products when H_2O_2 photodissociates, will not as likely escape the cage as the H from water in reaction (3), due to a stronger interaction with water molecules. Furthermore, the near equality of the observed and experimental concentration values also imply that the solid phase photo-destruction rate is comparable or smaller than destruction by the ions, and thus we consider only the characteristic lifetime calculated for ions. Newly exposed μm-layers of pristine ice would develop equilibrium concentrations in the characteristic time of 13 days estimated above and, because the equilibrium is of continual production and destruction, the mean life of surficial H_2O_2 molecules is the same. Note that changes in the magnetospheric flux will *not* change the surface concentration providing that the photodestruction rate is much smaller than the ion impact destruction rate.

We now compare the position and shape of Europa's 3.5-μm feature with laboratory absorbance spectra of irradiated samples. We used a low-noise NIMS reflectance spectrum R spatially averaged over Europa's leading side together with a cubic polynomial, R_c, fit to the "continuum" adjacent to the peroxide feature. The computed spectrum $[-\ln(R/R_c)]$ is proportional to the spectral absorptivity of H_2O_2 and is compared to laboratory spectra in Fig. 9. The position of Europa's feature agrees with the 80 K spectrum to within 0.01 μm and within the 0.015-μm instrumental uncertainty. The width and shape of the bands are also in good agreement. The spectral fit, coupled with consistency in the equilibrium concentrations, provide further evidence for extensive radiolytic processing on Europa.

5. Conclusions

Ion irradiation of pure ice with 50–100 keV protons and Ar^+ produces hydrogen peroxide in the explored temperature range: 20–120 K, which extends from close to the values for ice-coated interstellar grains to temperatures typical of icy satellites in the outer Solar System. Quantitative analysis of the 3.5-μm infrared absorption band, after non-linear background subtraction, shows that the concentration of H_2O_2 rises with irradiation fluence to a saturation level which, at 80 K, is very close to that found on Europa. Furthermore, the shape and position of the 3.5-μm band produced by ion irradiation also agrees well with that reported for Europa. The fact that Moore and Hudson (2000) could not detect hydrogen peroxide from pure ice radiolysed with 800 keV protons is explained by the known dependence of molecular synthesis on the density of energy deposition, which is much lower for 800 keV protons than in our experiments.

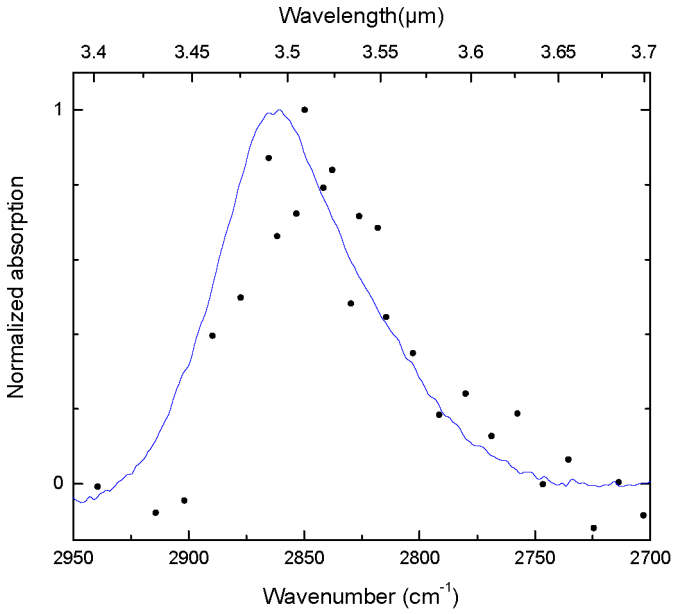

Fig. 9. A comparison of the 3.5-μm H_2O_2 absorption feature on Europa (circles) and that produced by 100 keV H^+ ion irradiation of water ice at 80 K (solid line).

Annealing of water ice irradiated at low temperatures to 120 K shows a slight irreversible upward shift in the transition frequency of the 3.5-μm band. After annealing to 120 K, the band has a different temperature dependence, this time reversible, and a shoulder appears at the low frequency side in the absorption band at lower temperatures. Annealing to temperatures where sublimation is important reveals that the produced H_2O_2 is relatively stable until the film desorbs from the substrate, and that it desorbs at a slower rate than water.

Acknowledgments

We would like to thank P. Schare for technical assistance and B.D. Teolis for useful discussions on thin-film IRRAS experiments. We acknowledge support for the NASA Cosmochemistry Program and from the Virginia Space Grant Consortium.

References

Alam, M.S., Kelm, M., Rao, B.S.M., Janata, E., 2004. Reaction of $H^\bullet$ with H_2O_2 as observed by optical absorption of perhydroxyl radicals or aliphatic alcohol radicals and of $^\bullet$OH with H_2O_2: A pulse radiolysis study. Rad. Phys. Chem. 71, 1087–1093.

Anbar, M., 1968. Water and Aqueous Solutions. In: Ausloos, P. (Ed.), Fundamental Processes in Radiation Chemistry. Wiley, New York, pp. 651–685.

Bahr, D.A., Fama, M.A., Vidal, R.A., Baragiola, R.A., 2001. Radiolysis of water ice in the outer Solar System: Sputtering and trapping of radiation products. J. Geophys. Res. E 106, 33285–33290.

Baragiola, R.A., Bahr, D.A., 1998. Laboratory studies of the optical reflectance and stability of oxygen on Ganymede. J. Geophys. Res. 103, 25865–25872.

Baragiola, R.A., Atteberry, C.L., Bahr, D.A., Peters, M., 1999a. Origin of solid oxygen on Ganymede, Reply to comment by R.E. Johnson on "Laboratory studies of the optical properties and stability of oxygen on Ganymede." J. Geophys. Res. 104, 14183–14187.

Baragiola, R.A., Atteberry, C.L., Bahr, D.A., Jakas, M.M., 1999b. Solid-state ozone synthesis by energetic ions. Nucl. Instr. Methods Phys. Res. B 157, 233–238.

Bednarek, J., Plonka, A., 1987. Single-crystal electron-spin resonance studies on radiation-produced species in the ice Ih. II. The HO_2 radicals. J. Chem. Soc. Faraday Trans. 83, 3725–3735.

Carlson, R.W., 2001. Spatial distribution of carbon dioxide, hydrogen peroxide, and sulfuric acid on Europa. Bull. Amer. Astron. Soc. 33, 1125.

Carlson, R.W., Anderson, M.S., Johnson, R.E., Smythe, W.D., Hendrix, A.R., Barth, C.A., Soderblom, L.A., Hansen, G.B., McCord, T.B., Dalton, J.B., Clark, R.N., Shirley, J.H., Ocampo, A.C., Matson, D.L., 1999. Hydrogen peroxide on the surface of Europa. Science 283, 2062–2064.

Cooper, J.F., Johnson, R.E., Mauk, B.H., Garrett, H.B., Gehrels, N., 2001. Energetic ion and electron irradiation of the icy Galilean satellites. Icarus 149, 133–159.

Cooper, P.D., Johnson, R.E., Quickenden, T.I., 2003. Hydrogen peroxide dimers and the production of O_2 in icy satellite surface. Icarus 166, 444–446.

Famá, M., Bahr, D.A., Teolis, B.D., Baragiola, R.A., 2002. Ion beam induced chemistry: The case of ozone synthesis and its influence on the sputtering of solid oxygen. Nucl. Instr. Methods Phys. Res. 193, 775–780.

Gerakines, P.A., Schutte, W.A., Ehrenfreund, P., 1996. Ultraviolet processing of interstellar ice analogs. Astron. Astrophys. 312, 289–305.

Gomis, O., Satorre, M.A., Strazzulla, G., Leto, G., 2004a. Hydrogen peroxide formation by ion implantation in water ice and its relevance to the Galilean satellites. Planet. Space Sci. 52, 371–378.

Gomis, O., Leto, G., Strazzulla, G., 2004b. Hydrogen peroxide production by ion irradiation of thin water ice films. Astron. Astrophys. 420, 405–410.

Hart, E.J., Platzman, R.L., 1961. Radiation chemistry. In: Errera, M., Forssberg, A. (Eds.), Mechanisms in Radiobiology. Academic Press, New York, pp. 99–120.

Hochanadel, C.J., 1960. Radiation chemistry of Water. In: Burton, M., Kirby-Smith, J.S., Magee, J.L. (Eds.), Comparative Effects of Radiation. Wiley, New York, pp. 151–189.

Hougen, J.T., 1984. Summary of group theoretical results for microwave and infrared studies of H_2O_2. Can. J. Phys. 62, 1392.

Huebner, W.F., Keady, J.J., Lyon, S.P., 1992. Solar photo rates for planetary atmospheres and atmospheric pollutants. Astrophys. Space Sci. 195, 1–293.

Johnson, R.E., Quickenden, T.I., Cooper, P.D., McKinley, A., Freeman, C.G., 2003. The production of oxidants in Europa's surface. Astrobiology 3, 823–850.

Khriachtchev, L., Pettersson, M., Jolkkonen, S., Pehkonen, S., Rasanen, M., 2000. Photochemistry of hydrogen peroxide in Kr and Xe matrixes. J. Chem. Phys. 112, 2187–2194.

Lin, C.L., Rohatgi, N.K., DeMore, W.B., 1978. Ultraviolet absorption cross sections of hydrogen peroxide. Geophys. Res. Lett. 5, 113–115.

Luñák, S., Sedlák, P., 1992. Photoinitiated reactions of hydrogen peroxide in the liquid phase. J. Photochem. Photobiol. A Chem. 68, 1–33.

Moore, M.H., Hudson, R.L., 2000. IR detection of H_2O_2 at 80 K in ion-irradiated laboratory ices relevant to Europa. Icarus 145, 282–288.

Nandi, D., Krishnakumar, E., Rosa, A., Schmidt, W.F., Illenberger, E., 2003. Dissociative electron attachment to H_2O_2: A very effective source for OH and OH^- generation. Chem. Phys. Lett. 373, 454–459.

Okabe, H., 1978. Photochemistry of Small Molecules. Wiley, New York.

Pan, X., Bass, A.D., Jay-Gerin, J.P., Sanche, L., 2004. A mechanism for the production of hydrogen peroxide and the hydroperoxyl radical on icy satellites by low-energy electrons. Icarus 172, 521–525.

Paranicas, C., Carlson, R.W., Johnson, R.E., 2001. Electron bombardment of Europa. Geophys. Res. Lett. 28, 673–676.

Paranicas, C., Ratliff, J.M., Mauk, B.H., Cohen, C., Johnson, R.E., 2002. The ion environment near Europa and its role in surface energetics. Geophys. Res. Lett. 29, 181–184.

Pastina, B., LaVerne, J.A., 2001. Effect of molecular hydrogen on hydrogen peroxide in water radiolysis. J. Phys. Chem. 105, 9316–9322.

Pettersson, M., Tuominen, S., Rasanen, M., 1997. IR spectroscopic study of H_2O_2, HDO_2, and D_2O_2 isolated in Ar, Kr, and Xe matrices. J. Phys. Chem. 101, 1166–1171.

Plonka, A., Szajdzinska-Pietek, E., Kroh, J., 1984. Decay kinetics of hydroxyl radicals in frozen aqueous systems. Radiat. Phys. Chem. 23, 583–587.

Sack, N.J., Baragiola, R.A., 1993. Sublimation of vapor-deposited water ice below 170 K, and its dependence on growth conditions. Phys. Rev. B (Condensed Matter) 48, 9973–9978.

Siegel, S., Flournoy, J.M., Baum, L.H., 1961. Irradiation yields of radicals in gamma-irradiated ice at 4.2 and 77 K. J. Chem. Phys. 34, 1782–1788.

Sieger, M.T., Simpson, W.C., Orlando, T.M., 1998. Production of O_2 on icy satellites by electronic excitation of low-temperature water ice. Nature 394, 554–556.

Slanger, T.G., Black, G., 1982. Photodissociative channels at 1216 Å for H_2O, NH_3, and CH_4. J. Chem. Phys. 77, 2432–2437.

Spencer, J.R., Calvin, W.M., 2002. Condensed O_2 on Europa and Callisto. Astron. J. 124, 3400–3403.

Spencer, J.R., Tamppari, L.K., Martin, T.Z., Travis, L.D., 1999. Temperatures on Europa from Galileo PPR: Nighttime thermal anomalies. Science 284, 1514–1516.

Spinks, J.W.T., Woods, R.J., 1990. An Introduction to Radiation Chemistry. Wiley, New York.

Vidal, R.A., Bahr, D., Baragiola, R.A., Peters, M., 1997. Oxygen on Ganymede: Laboratory studies. Science 276, 1839–1842.

Wasselin-Trupin, V., Baldachhino, G., Bouffard, S., Hickel, B., 2002. Hydrogen peroxide yields in water radiolysis by high-energy ion beams at constant LET. Radiat. Phys. Chem. 65, 53–61.

Westley, M.S., Baratta, G.A., Baragiola, R.A., 1998. Density and index of refraction of water ice films vapor deposited at low temperatures. J. Chem. Phys. 108, 3321–3326.

Zahnle, K., Dones, L., Levison, H.F., 1998. Cratering rates on the Galilean satellites. Icarus 136, 202–222.

Ziegler, J.F. 2003. Stopping and Range of Ions in Matter, SRIM 2003, available at www.srim.org.